Talanta 186 (2018) 354–361

Contents lists available at ScienceDirect

Talanta

journal homepage: www.elsevier.com/locate/talanta

Fast and reliable BIA/amperometric quantification of acetylcysteine using a nanostructured double hydroxide sensor

Anabel Laza Correa[a], Josué M. Gonçalves[a], Pamela O. Rossini[a], Juliana S. Bernardes[b], Carlos A. Neves[c], Koiti Araki[a], Lucio Angnes[a,*]

[a] Department of Fundamental Chemistry, Institute of Chemistry, University of Sao Paulo, Av. Prof. Lineu Prestes 748, Sao Paulo, SP 05508-000, Brazil
[b] Brazilian Nanotechnology National Laboratory (LNNano), Brazilian Center for Research in Energy and Materials (CNPEM), Zip Code 13083-970, Campinas, São Paulo, Brazil
[c] Faculdade de Química - Instituto de Ciências Exatas e Naturais - Universidade Federal do Pará. Rua Augusto Corrêa, 01 - Guamá. CEP 66075-110 Belém, Brazil

ARTICLE INFO

Keywords:
Nanoparticles
Nanostructured electrode
Electrocatalysis
Nickel hydroxide
Amperometric sensor
N-acetylcysteine, Batch injection analysis (BIA)

ABSTRACT

This study reports the preparation and characterization of nickel/lead hydroxide nanoparticles used to construct electrochemical sensors, which were investigated for amperometric quantification of N-acetylcysteine (NAC). The newly synthesised material presents good uniformity, with the lead (II) ions homogenously incorporated into the alpha nickel hydroxide crystal structure, confirmed by X-ray diffraction, transmission electron microscopy and X-ray photoelectron spectroscopy analyses. Films of nanoparticles (3 nm in size) were prepared on conductive fluorine-doped tin oxide-coated glass slides and used connected to a specially built batch injection analysis (BIA) cell with a capacity of only 4 mL and the electrode positioned in the bottom. To attain optimal analytical performance, the main parameters for BIA measurements (volume injected, different velocities of injection and best distance of the pipette from the electrode) were evaluated, as was the working potential, to determine the optimal conditions. Linear responses were obtained for the concentration range from 20 to 220 μmol L^{-1}, and the limits of detection (3σ/slope) and quantification (10σ/slope) were calculated as 0.23 μmol L^{-1} and 0.70 μmol L^{-1}, respectively. The new NAC sensor does not exhibit a memory effect and has enormous potential utility in the quantitative determination of N-acetylcysteine in drugs. The results of the analysis of NAC obtained using BIA presented good concordance with those obtained by chromatography. The analytical frequency attained using BIA (120 analysis h^{-1}) compares very favourably with the one obtained using chromatography (6 analysis h^{-1}).

1. Introduction

N-Acetylcysteine (NAC) is the *N*-acetyl derivative of L-cysteine, a precursor in the biosynthesis of the antioxidant species glutathione, whose sulfhydryl group has the capacity to reduce free radicals [1]. The main use of this compound is in the treatment of respiratory disorders, such as acute bronchitis and chronic pulmonary disease, as NAC acts to loosen and facilitate the expulsion of mucus [2,3]. The common administration routes of NAC are oral (tablets or syrups), injectable and as an aerosol. More recently, it was discovered that NAC is effective in the treatment of paracetamol overdose [4], and its inhibitory effect on virus replication was also demonstrated [5]. In addition, due to its antioxidant and anti-inflammatory characteristics, many properties have been attributed to NAC, but the opinions of specialists are controversial. For example, it was recommended as a dietary supplement [6], as protection in cases of ingestion of radioactive contrast agents [7], in the treatment of psychiatric diseases [8] and even suggested as an anticancer agent [9], but this last suggestion was ruled out by another study demonstrating the opposite characteristics [10].

Several different techniques can be used to quantify NAC, such as spectrophotometry [11], electrophoresis [12,13], turbidimetry [14] and conductometry [15], but the utilization of liquid chromatography (mainly HPLC) is the most common [16–19]. Some of these methods present limitations such as low frequency of analysis, generation of organic residues and elevated costs. In addition, NAC can degrade rapidly [12,16]; therefore, methods requiring minimal sample manipulation are desirable. Electroanalytical techniques are an attractive alternative for the analysis of drugs because they combine good precision and high frequency of analysis [20,21], two highly relevant characteristics, particularly when considering that NAC is not very stable in solution.

The advent of modified electrodes has remarkably increased the

* Corresponding author.
E-mail address: luangnes@iq.usp.br (L. Angnes).

https://doi.org/10.1016/j.talanta.2018.04.053
Received 16 January 2018; Received in revised form 10 April 2018; Accepted 18 April 2018
Available online 23 April 2018
0039-9140/

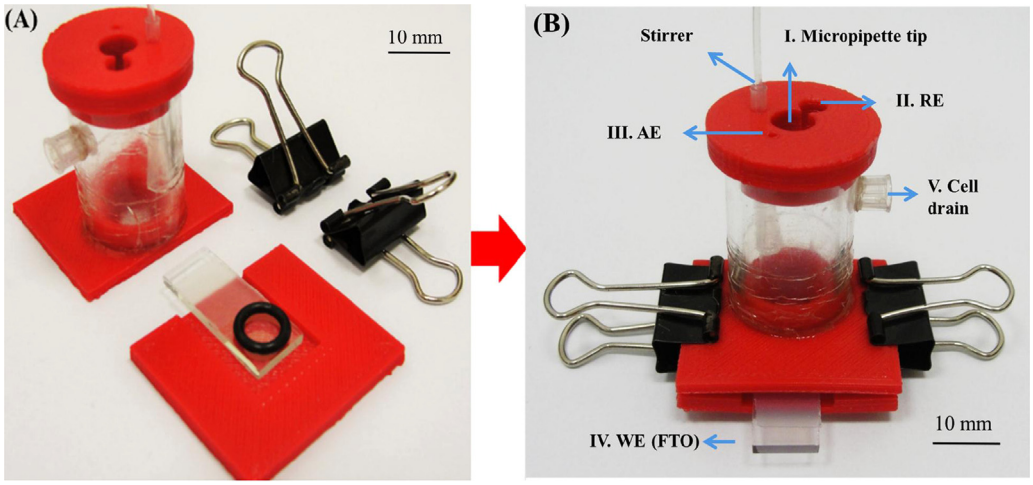

Fig. 1. (A) Parts of the BIA cell showing the FTO electrode and the o-ring to avoid solution leakage; (B) assembled BIA cell showing the orifices for I) motorized micropipette, II) reference electrode, and III) auxiliary electrode IV) FTO working electrode, and V) the cell drain.

possibilities of developing tailored devices for a specific application with elevated sensitivity and selectivity for the quantification of target analytes. The modification of the electrode surface with suitable electrochemically and electrocatalytically active materials can provide lower oxidation potentials and higher selectivity, avoiding fouling and consequent inactivation of the electrode surface. In this context, the utilization of nanoparticles offers additional advantages associated with the huge increase in the electroactive surface area, producing a considerable increase in the electrochemical kinetics [22,23].

In our laboratory, the utilization of nanoparticles constituted by two different metals to modify electrodes is in progress. In a previous study [24], Ni/Co nanoparticles were explored for the quantification of isoniazid where the oxidation potential of that pharmaceutical compound was demonstrated to be tuneable by the relative amounts of those metal ions. Also, it was demonstrated that mixed Ni/Ce hydroxides are more stable than the respective nickel hydroxide nanoparticles, and an electrode modified with this material was successfully employed for catalytic oxidation and quantification of prednisone [25].

In the present study, we take advantage of the electrocatalytic characteristics of the double hydroxide constituted by Ni (75%) and Pb (25%), now represented simply as $Ni_{1-x}Pb_x(OH)_2$. In the next sections are described the details of preparation and characterization of the nanomaterial itself, preparation of electrodes and an innovative design of the amperometric cell for batch injection analysis (BIA) measurements and its utilization for the quantitative determination of N-acetylcysteine contained in injectable ampoules.

2. Experimental

2.1. Reagents

Analytical grade reagents were utilized as received in this work. Nickel acetate, lead nitrate, anhydrous glycerine, *n*-butyl alcohol, hydrochloric acid, acetonitrile and phosphoric acid were acquired from Sigma and Merck. Potassium hydroxide was purchased from Synth. Aqueous solutions were prepared with water (R ≥ 18.2 MΩ cm) filtered and purified in a Milli-Q water purification system (Millipore Bedford MA, USA). FTO glass slides with the dimensions 25 × 10 × 2 mm (resistivity 15 Ω/cm^2 Pilkington Tech-15) were purchased from Pilkington in Brazil. Injectable ampoules of assorted brands were purchased in drugstores and used after dilution with the electrolyte.

2.2. Syntheses

Two different nanoparticles were prepared (nickel hydroxide and nickel-lead mixed hydroxides) utilizing the modified Tower method [26,27]. To prepare $Ni(OH)_2$ nanoparticles, 9.64 mmol of nickel acetate was dissolved in 25 mL of glycerol, and the appropriate quantity of potassium hydroxide (dissolved in *n*-butanol) was added drop by drop to that mixture to produce $Ni(OH)_2$. The mixed hydroxide material was prepared by dissolving 7.23 mmol of nickel acetate and 2.41 mmol of lead nitrate (75%:25% molar proportion) in 25 mL of glycerol, and the mixture was reacted with KOH solution as described above to obtain the expected $Ni_{(0.75)}Pb_{(0.25)}(OH)_2$ nanoparticles.

2.3. Characterization

The samples were characterized by X-ray diffractometry (XRD) in a Bruker D2 Phaser instrument, equipped with a Cu Kα source (λ = 1.5418 Å, 30 kV, 15 mA, step = .05°) in the 2θ range from 5° to 70°. The surface composition of hydroxide nanoparticles was analysed by X-ray photoelectron spectroscopy (XPS), using a K-Alpha X-ray photoelectron spectrometer (Thermo Fisher Scientific, UK) equipped with a hemispherical electron analyser and monochromatic Al Kα (1486.6 eV) radiation. Survey (full-range) and high-resolution spectra for Pb and Ni were respectively acquired using pass energy of 200 and 50 eV. Curve-fitting analyses were carried out using the Thermo Advantage Software (Version 5.921). The XPS results presented in this work correspond to an average of at least three independent measurements performed in different regions of each sample.

Transmission electron microscopy (TEM) images of nanocomposites were obtained in a JEOL JEM-2100-F microscope at an accelerating voltage of 200 kV. Samples were prepared on 400-mesh copper grids with lacey carbon film coating (Ted Pella) by dispersing 3 µL of $Ni_{0.75}Pb_{0.25}(OH)_2$ @GO suspension diluted with water.

Amperometric and voltammetric measurements were accomplished with a µAutolab Type III Potentiostat/Galvanostat (Metrohm Autolab, Utrecht, The Netherlands) using a three-electrode cell. A Shimadzu HIC-6A HPLC was used for chromatographic analyses. Parts of the BIA cell (shown in red, Fig. 1) were constructed in ABS using a low-cost 3D printer (Rip Rap Prusa i3, with a 0.4-mm extruder nozzle) operating at 230 °C, and to design these parts, the open program OpenSCAD was utilized.

2.4. Preparation of modified electrodes

FTO glass sheets were used in this study to build the modified electrodes, as they can withstand the thermal treatment (240 °C) necessary to eliminate most of the glycerine from the material. To perform the preliminary experiments, we developed a way to define the

electrode area. This was done by protecting the desired surface area with an adhesive paper cut with a 3D laser printer. The uncoated region of the FTO glass sheet was eroded by sandblasting in order to define FTO circular electrodes (∅ = 6 mm) connected by a narrow line to a strip on the opposite edge used as an electric contact. Most of the contact line was protected again with nail polish after removal of the adhesive paper. Finally, 20 μL of a colloidal dispersion of nanoparticle (sol) was transferred to the circular electrode area and spin coated (2000 rpm) for 1 min, generating a homogeneous film. This procedure was repeated once more, and then the electrodes were kept in a furnace at 240 °C, for 2 h. This procedure was not necessary for the electrodes utilized for BIA experiments, which were entirely modified. The electrode area was defined by the O-ring utilized in the bottom of the cell (as shown in Fig. 1).

2.5. Electrochemical measurements

All electrochemical experiments were performed in a specially designed BIA cell, the base and cover of which were constructed of ABS (acrylonitrile-butadiene-styrene), using a 3D printer, to fit tightly into a Plexiglass® tube used as the cell body, as depicted in Fig. 1. The working electrode (designed on an FTO glass sheet) was positioned in the centre of the cell base and pressed by two paper clamps. The O-ring prevented leakage of the internal solution and defined the BIA electrode area. A hole was drilled in the centre of the cover, in such a way as to position the automatic micropipette exactly in the centre of the FTO electrode. The reference electrode (Ag/AgCl $_{KCl\ 3.0\,mol\,L^{-1}}$) and the auxiliary electrode (Pt) were positioned at two additional holes drilled in the cell cover. The solution was stirred using a flexible plastic tube connected to the axis of a small electric motor, the rotation of which was controlled by the voltage applied to it. The total volume of this cell was 4.5 cm^3 and the volume of the solution was approximately 4 mL. At the side of the Plexiglass® body of the cell, a drain was connected to remove the excess solution.

3. Results and discussion

3.1. Material characterization

The surface composition of the hydroxide samples was determined by XPS measurements. Fig. 2A shows the atomic percentage of each element; the Ni:Pb atomic ratio for α-Ni_{1-x} $Pb_x(OH)_2$ was found to be 76:24, in good agreement with the results acquired by ICP-OES (bulk composition, 74.7:25.3), suggesting that the material, bulk and its surface, had the same composition. The presence of carbon can be attributed to residual glycerine molecules and acetate ions as well as adventitious carbon layers. This uniformity was expected, as the solubility constants of $Ni(OH)_2$ and $Pb(OH)_2$ are very similar, and the precipitation of both metals occurred simultaneously.

High-resolution Ni_2p spectra (Fig. 2B) of α-$Ni(OH)_2$ and α-$Ni_{1-x}Pb_x(OH)_2$ were compared with that of a reference $Ni(OH)_2$ sample (black line) and all exhibited very similar spectral profiles. Pb4f curves of α-$Ni_{1-x}Pb_x(OH)_2$ were plotted together with the Pb4f from PbO_2 and Pb_3O_4 reference samples (Fig. 2C). The observed α-$Ni_{1-x}Pb_x(OH)_2$ peaks were symmetrical and had a well-separated spin-orbit (ca 4.8 eV). Furthermore, the binding energy was closer to that of the Pb_3O_4 reference, indicating that the α-$Ni_{1-x}Pb_x(OH)_2$ sample contained mixed lead oxides [28]. Lead dioxide has metallic properties, probably caused by oxygen vacancies, thus presenting a lower biding energy (BE) than Pb_3O_4 and native lead oxide (PbO) [29].

The X-Ray diffractograms of the $Ni(OH)_2$ and $Ni_{1-x}Pb_x(OH)_2$ nanoparticles seem to confirm the above hypothesis, exhibiting very similar spectral profiles characterized by three low-intensity and broad signals at 8° (300), 34° (101) and 62° (110), characteristic of a material in the α-phase [30]. The interplanar distances in α-$Ni(OH)_2$ and α-$Ni_{1-x}Pb_x(OH)_2$ were determined, using the Bragg equation, to be 8.92 and 8.84 Å, respectively. The structural effect of lead ions seems to be quite small, and no peaks assignable to pure PbO_x crystals could be found in the diffractogram of the mixed hydroxide material, suggesting an isomorphic substitution of lead into the nickel hydroxide structure.

However, lead can be found in the 2 + and 4 + oxidation states forming compounds such as $Pb^{II}(OH)_2$/$Pb^{II}O$ and $Pb^{IV}O_2$ but also Pb_3O_4, a mixed oxide containing 2Pb(II):Pb(IV). Considering the possibility of reticular substitution of Ni(II) ions by lead ions in the turbostatic alpha phase structure, Pb(IV) seems to fit better than Pb(II) considering its smaller size. However, when 9.64 mmol of lead nitrate was dissolved in 25 mL of glycerol and reacted with KOH solution, following the same procedure used for preparation of $Ni(OH)_2$ and α-$Ni_{1-x}Pb_x(OH)_2$ nanoparticles, a dark solution was formed instead of a white or colourless suspension. The XRD and XPS data obtained from the dark powder obtained upon washing with water and drying in a muffle at 180 °C, are shown in Fig. 2. These results are consistent with Pb_3O_4 according to the analysis by DRX, or a mixture of PbO_2 and Pb_3O_4 considering the XPS spectrum which exhibited Pb_{4f} peaks with binding energies in between those materials. Surprisingly, though, the Pb_{4f} peaks found for α-$Ni_{1-x}Pb_x(OH)_2$ presented quite distinct binding energies, more consistent with the presence of lead as $Pb(OH)_2$, in fact generating a mixed hydroxide nanomaterial. Accordingly, the possibility of its incorporation into the larger interstitial sites of the alpha nickel hydroxide structure cannot be ruled out. The unusual stabilization of lead(II) hydroxide awaits further study but probably can be attributed to some kind of matrix effect, which may be reflected in its thermal behaviour, as detailed below.

Thermal analysis (STA, DTA-TG-DTG) was performed at 25–700 °C for both pure and mixed hydroxides [see Fig. S1]. α-$Ni(OH)_2$ exhibited three endothermic peaks, of which the first two occurred at relatively low temperatures (75 and 220 °C) with minor mass loss, whereas the third one took place at 359 °C with a major variation in mass. The first two events were attributed to the elimination of weakly and strongly bonded water molecules, as well as some other species, such as acetate, present as counter-ions in the reactants used in the synthesis. The wide variation observed at 359 °C for $Ni(OH)_2$ suggests the elimination/decomposition of glycerine, such as in the transformation of the metal hydroxides into their respective oxides. For α-$Ni_{1-x}Pb_x(OH)_2$, the decrease in mass in the 25–220 °C region was less pronounced, and the third event occurred in the same temperature region but in two well-defined steps culminating in a very sharp mass loss event at 371 °C. The DTG of both curves shows a smaller variation in mass in the case of α-$Ni_{1-x}Pb_x(OH)_2$, suggesting a smaller amount of glycerine in this nanomaterial.

Samples for transmission electron microscopy (TEM) analysis were prepared by first covering graphene oxide (GO) sheets with α-$Ni_{1-x}Pb_x(OH)_2$ nanoparticles and then depositing this nanocomposite on a lacey carbon support film (PELCO®). As shown in Fig. 3A, round-to-oval-shaped 2–3 nm nanoparticles were found, confirming the presence of small nanoparticles. A closer inspection by HRTEM indicated they had a high degree of crystallinity, as confirmed by the reflection fringes (Figs. 3B and 3C) assigned to the 200 plane of NiO (JCPDS n° 73–1523).

The conversion of α-$Ni_{1-x}Pb_x(OH)_2$ to $Ni_{1-x}Pb_xO$ induced by the electron beam is favoured by the high vacuum in the microscope chamber [31], generating oxide nanoparticles 2–3 nm in diameter.

3.2. Electrochemical characterization

Cyclic voltammetry was used to study the electrochemical behaviour of electrodes modified with the α-$Ni_{1-x}Pb_x(OH)_2$ nanoparticles. The as-prepared electrodes tend to exhibit anodically shifted low-intensity oxidation waves, but 30 successive cycles at 0.15–0.65 V, in 1 mol L^{-1} KOH solution (at 20 mV s^{-1}), are enough to condition the electrodes, generating stable and enhanced voltammetric responses. The voltammograms present two peaks (one anodic and another cathodic) attributed to the oxidation and reduction of nickel ions

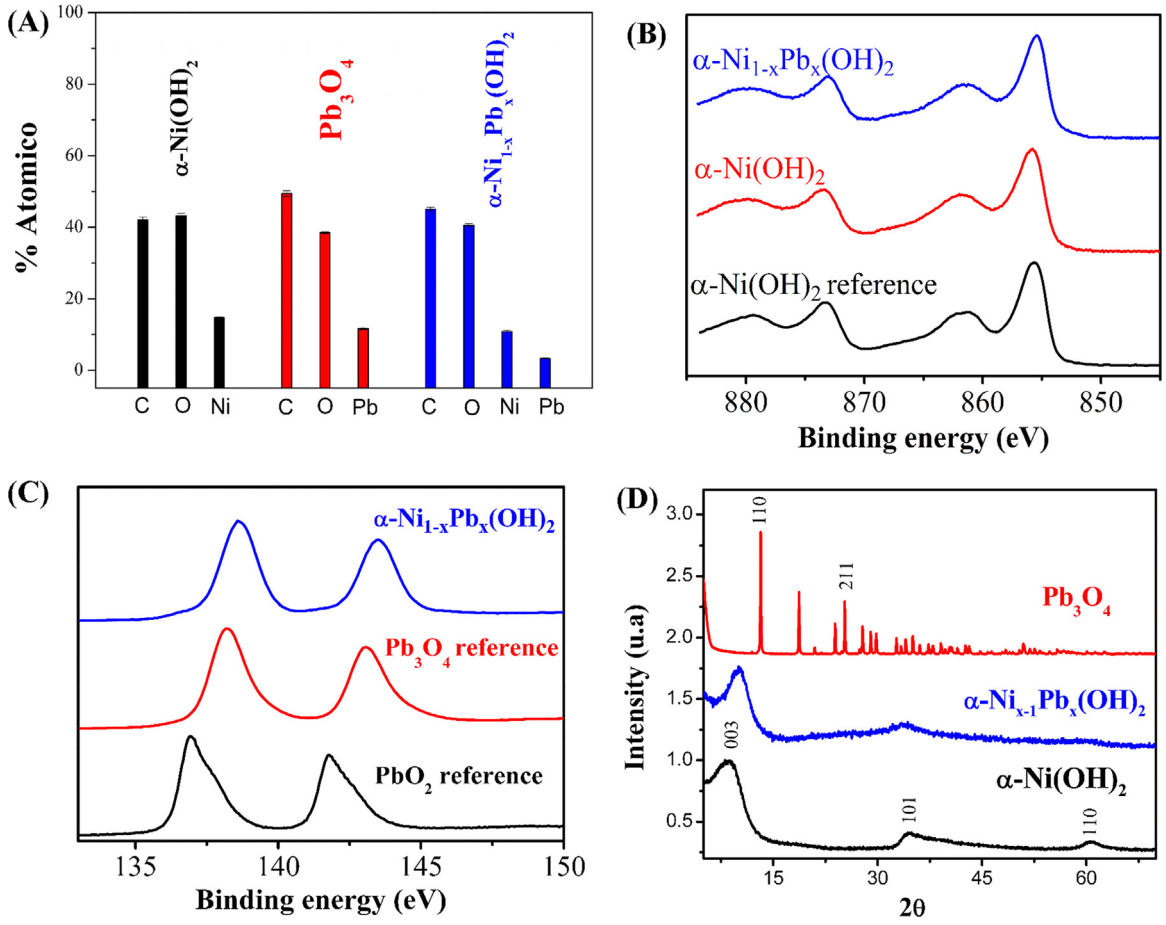

Fig. 2. Comparative X-ray photoelectron spectra of α-$Ni_{1-x}Pb_x(OH)_2$, α-$Ni(OH)_2$, Pb_3O_4 and PbO_2. (A) Atomic percentage of C, O, Ni and Pb determined from survey XPS spectra of α-$Ni_{1-x}Pb_x(OH)_2$, α-$Ni(OH)_2$, and Pb_3O_4, (B) Ni_{2p} and (C) Pb_{4f} high resolution XPS spectra, and (D) X-Ray diffractograms of α-$Ni(OH)_2$, α-$Ni_{1-x}Pb_x(OH)_2$ and Pb_3O_4 in the 5 a 70° 2θ range.

($Ni^{3+/2+}$ redox pair), as represented in the Eq. (1).

$$NiOOH + H_2O + e^- \leftrightarrow Ni(OH)_2 + OH^- \quad (1)$$

Both the pure and the mixed hydroxide materials present similar voltammetric profiles (Fig. 4) and good electrochemical responses after 300 consecutive redox cycles, but some differences can be easily noticed. The voltammogram of the electrode modified with α-$Ni_{1-x}Pb_x(OH)_2$ nanoparticles presents narrower waves and smaller anodic and cathodic peak potential difference (ΔE_{NiPb} = 0.20 V) than the electrodes modified with α-$Ni(OH)_2$ nanoparticles (ΔE_{Ni} = 0.24 V), as expected for a more conductive material. The faster charge transfer processes in the mixed hydroxide NPs, as compared with the pure nickel hydroxide, probably can be attributed to a diminution of the proton diffusion resistance [32].

3.3. Oxidation of NAC on FTO-α-$Ni_{1-x}Pb_x(OH)_2$

Organic molecules containing redox site(s), such as sulphides, phenols and catechols, are generally quite resistant to reduction and oxidation. In fact, NAC presents a high overpotential for oxidation

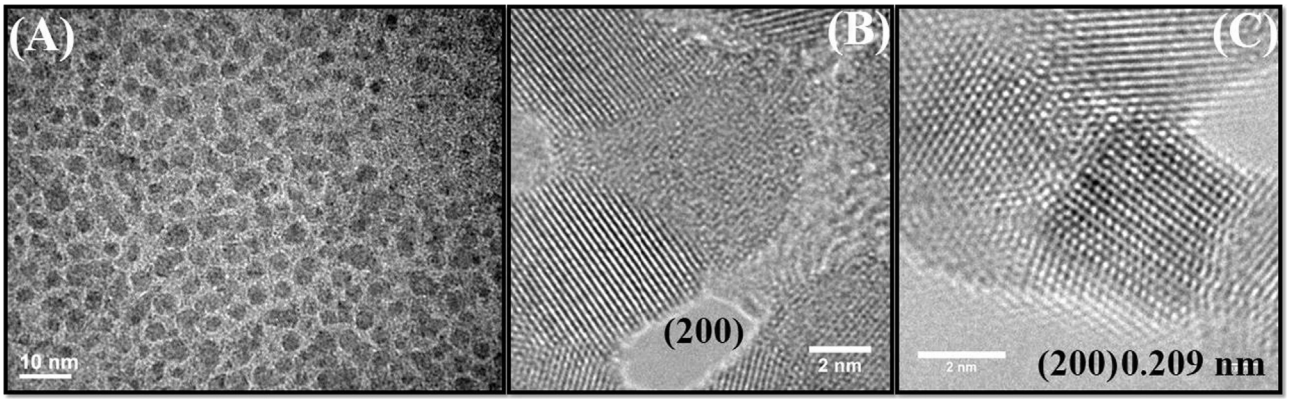

Fig. 3. (A) CTEM images of a densely packed layer of α-$Ni_{1-x}Pb_x(OH)_2$ nanoparticles deposited on GO sheets; and (B-C) corresponding HRTEM images after a dehydroxylation reaction induced by the electron beam generating the respective mixed oxide nanoparticles.

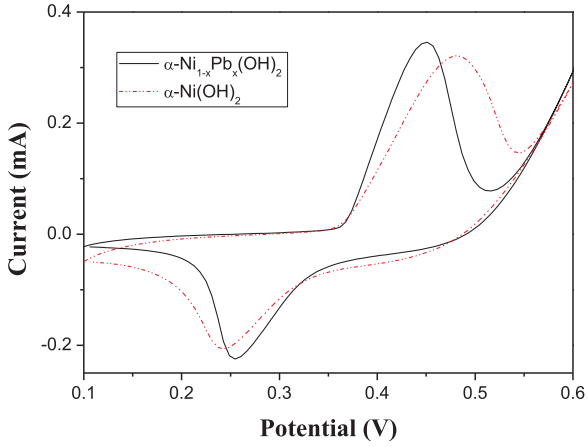

Fig. 4. Cyclic voltammograms of α-$Ni_{1-x}Pb_x(OH)_2$ (black line) and α-$Ni(OH)_2$ (red line) in 1.0 mol L^{-1} KOH, scan rate = 20 mV s^{-1}, after 300 successive redox cycles.

reactions on solid electrodes [33]. In the literature, most studies are focused on the quantification of NAC in discrete solutions based on carbon paste electrodes [34–39], glassy carbon electrodes [40–45] and other substrates [46–49], always containing one or more catalytic materials. Only two studies based on voltammetric detection under flowing conditions were previously developed [46,48]. The first one was developed in our laboratory [46] and was based on pyrolytic graphite modified with CoPC. Under this electrode, the porphyrin was much more stable than on other substrates. The other study [48] describes the utilization of a boron-doped diamond electrode. In the present study, FTO modified with α-$Ni_{0.75}Pb_{0.25}(OH)_2$ NPs was found to present a good electrocatalytic property and an amperometric response to NAC oxidation, as can be seen in Fig. 5.

Cyclic voltammetry studies show a redox peak of the electrode in KOH solution and a clear increase of the oxidation signal in the presence of NAC, at around 0.40 V (Fig. 5-A). Based on these results, BIA-amperometric experiments were performed at 0.40 V, generating a linear amperometric response up to 0.6 mmol L^{-1}. In this last experiment, a series of 12 successive additions of 0.05 mmol L^{-1} of NAC (0.01 mol L^{-1}, 20 µL, in KOH 1.0 mol L^{-1}) were performed while the solution was stirred, and the resulting signals are depicted in Fig. 5-B. The volume of solution inside the cell was 4.0 mL, and the additional volumes were drained through the lateral tube. Both, α-$Ni(OH)_2$ and α-$Ni_{1-x}Pb_x(OH)_2$ modified electrodes exhibited excellent and comparable amperometric responses to NAC oxidation, with a preference for the second one at larger concentrations. It is easy to observe that the FTO electrode gives no response at all, even at the highest concentrations of NAC at 0.4 V, the current onset being found at 0.5 V (inset of Fig. 5-A). Thus, the measured current can be entirely assigned to the oxidation of that analyte. It is important to point out that the limit of detection attained in the present study is not the lower one described in the literature (ex: see ref. 39,49) but is adequate for utilization under flowing conditions providing elevated frequency of analysis. Spectrophotometric determinations of NAC under a flowing regime were also described [50,51]. Both studies present the advantage of providing a larger throughput of analysis, but the disadvantage of requiring that other reagents be injected in the flowing stream to react with NAC. The fact that amperometric methods do not require any reagent for the analysis is a great advantage. In addition, in most pharmaceutical products, NAC is present at high concentrations and thus, a very low detection limit is not necessary.

3.4. Optimization of BIA parameters

The FTO-modified electrodes present a significant potential window: from − 1.2–0.6 V (not shown), but in the present study the region where NAC is oxidized, situated between − 0.15 and 0.60 V, was explored, because oxidation occurs close to 0.40 V. To elicit the best working potential for determination of NAC, hydrodynamic experiments were in the potential region situated in the interval of 0.25–0.49 V. Fig. 6-A presents the experimental results obtained by recording the amperometric response after injection of 50 µL of 0.1 mmol L^{-1} NAC solution while setting the potential to 0.25, 0.28, 0.31, 0.34, 0.37, 0.40, 0.43, 0.46 and 0.49 V in order to determine the best potential for analyses. All experiments were carried out in triplicate and the average current measured at each potential plotted as a function of potential for three identical assays indicated as time, as shown in Fig. 6-B. A sigmoidal response profile was found under the BIA regime where the current increased gradually from 0.25 to 0.34 V, much more rapidly from 0.37 to 0.40 V and after this, increased slowly. The additional increase in current (0.49 V and at more positive potentials) can be assigned to the oxidation of the solvent, an unfavourable condition for electroanalytical applications.

The optimization of other relevant parameters was carried out to find the best conditions for NAC quantification by BIA amperometric detection. The maximum capacity of the cell is only 4 mL, and the working electrode is situated in the bottom, such that the geometry

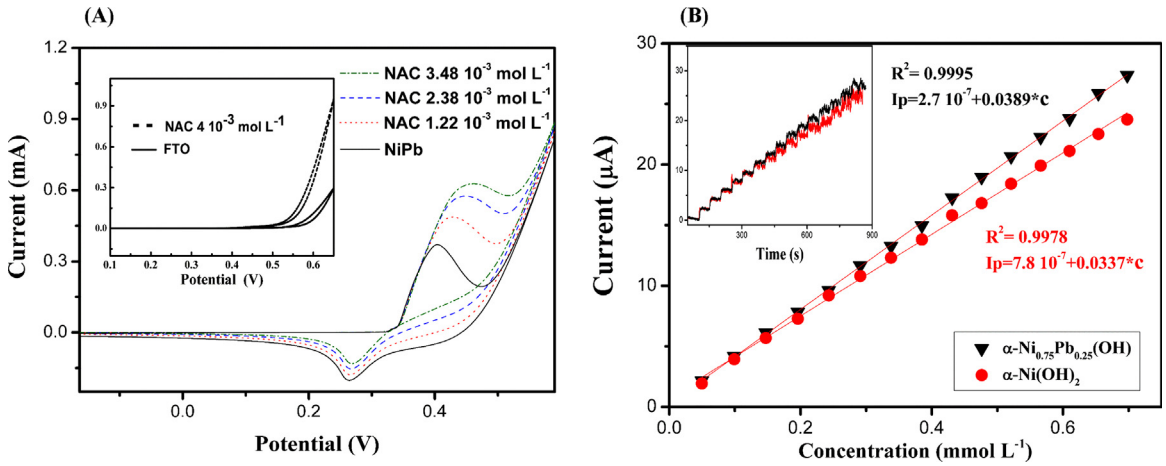

Fig. 5. (A) Cyclic voltammograms (20 mV s^{-1}) of a FTO electrode modified with α-$Ni_{1-x}Pb_x(OH)_2$ nanoparticles in neat electrolyte solution and after injection of 100 µL of NAC (0.05 mol L^{-1}) Inset: CVs of a clean FTO electrode in 1.0 mol L^{-1} KOH and after addition of 4 mmol L^{-1} of NAC. (B) Amperometric response (at fixed potential of 0.40 V vs. Ag/AgCl ($_{KCl\ 3.0\,mol\,L^{-1}}$)) for increasing concentrations of NAC using an FTO electrode modified with of α-$Ni(OH)_2$ (red line) and α-$Ni_{1-x}Pb_x(OH)_2$ (black line) nanoparticles after successive additions of 5 × 10^{-5} mol L^1 NAC solution on 1.0 mol L^{-1} KOH electrolyte solution.

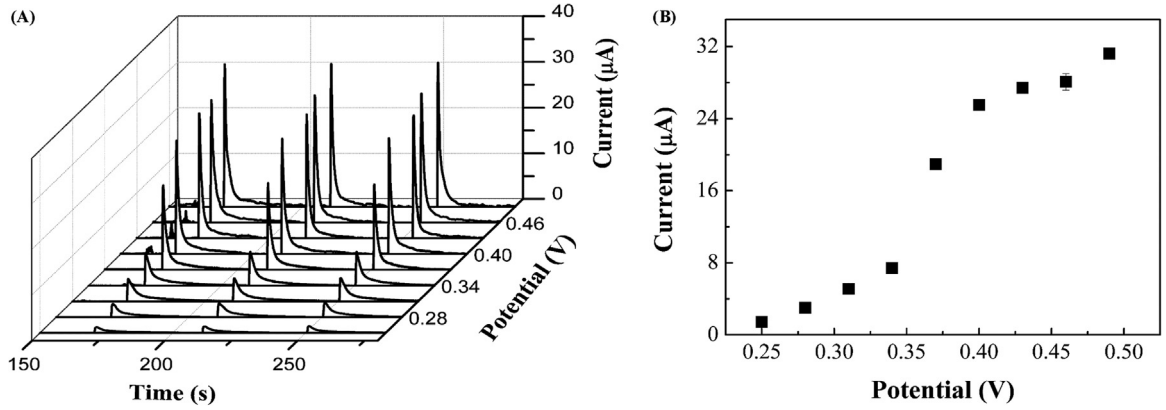

Fig. 6. (A) Three-dimensional plot showing BIA-amperograms as a function of potential (0.25–0.49 V vs. Ag/AgCl ($_{KCl\ 3.0\ mol\ L^{-1}}$) range) upon successive injections of 50 μL of 0.1 mmol L^{1} NAC solution in 4 mL of 1.0 mol L^{-1} KOH electrolyte solution. (B) Plot of the average current of three identical BIA assays depicted in (A) as a function of the applied potential.

Table 1
Optimized parameters for BIA analysis of NAC.

Parameter	Studied range	Optimized conditions
E_{app}	.25–0.49 V	0.40 V
tip-electrode distance	1–6 mm	3 mm
injection volume	20–80 μL	50 μL
injection rate	35–274 μL s^{-1}	274 μL s^{-1}

does not favour rapid dispersion of the injected analyte solution. Thus, a mechanical stirrer was used to obtain sharp differential amperometric responses and increase the sampling rate. The effect of parameters such as the distance of the pipette tip from the electrode surface, injection rate and injected volume was also evaluated and optimized (Fig. S2). The amperometric BIA response increased as a function of the injection rate and injection volume, reaching saturation around 274 μL s^{-1} and 50 μL, respectively. The best tip-to-electrode distance was found to be situated at 2–3 mm [52,53], where a maximum signal was observed. The optimized parameters are listed in Table 1.

Good repeatability (RSD = 1.9%; n = 40), analytical frequency (120 analyses h^{-1}) and sensibility for quantitative NAC determination was obtained using the optimized conditions (Fig. S3). An interesting linear dynamic range from 20 to 220 μmol L^{-1} (r^2 = 0.9996) was also realized, demonstrating the suitability of our amperometric BIA method, whose calibration curve is described by the equation I_p = 1.7 10^{-6} + 0.14 [NAC].

3.5. Determination of NAC in pharmaceutical samples

After optimization of all parameters and construction of the calibration curve, the proposed method was applied to the determination of NAC in pharmaceutical samples. The BIA amperograms obtained for injection of four NAC standard solutions in an increasing concentration sequence (a-d, 50–200 μmol L^{-1}), two different samples of injectable solutions of NAC, and the same standard solutions in a decreasing concentration sequence are shown in Fig. 7. The symmetry of the BIA-amperogram profile indicates that there is no memory effect, as confirmed by the matching corresponding current intensities and the linear increase in current as a function of concentration in both increasing and decreasing portions intercalated by the responses for the real samples S_1 and S_2. The limit of detection (3σ/slope) and the limit of quantification (10σ/slope) were determined to be 0.23 μmol L^{-1} and 0.70 μmol L^{-1}, respectively.

The results were validated by HPLC (Fig. S4), the standard method recommended by the Brazilian Pharmacopeia [54]. Very similar results were obtained by BIA and HPLC: 104.8 ± 0.4 and 106.0 ± 0.4 mg mL^{-1}, respectively, indicating exactness and precision similar to that obtained with the standard method, but with the advantage of being faster and less costly. The results obtained for NAC quantification in injectable pharmaceutical solutions by BIA and the standard HPLC method are compared in Table 2.

As demonstrated by the results, the quantification of NAC in commercial drugs using BIA is rapid and precise, producing results

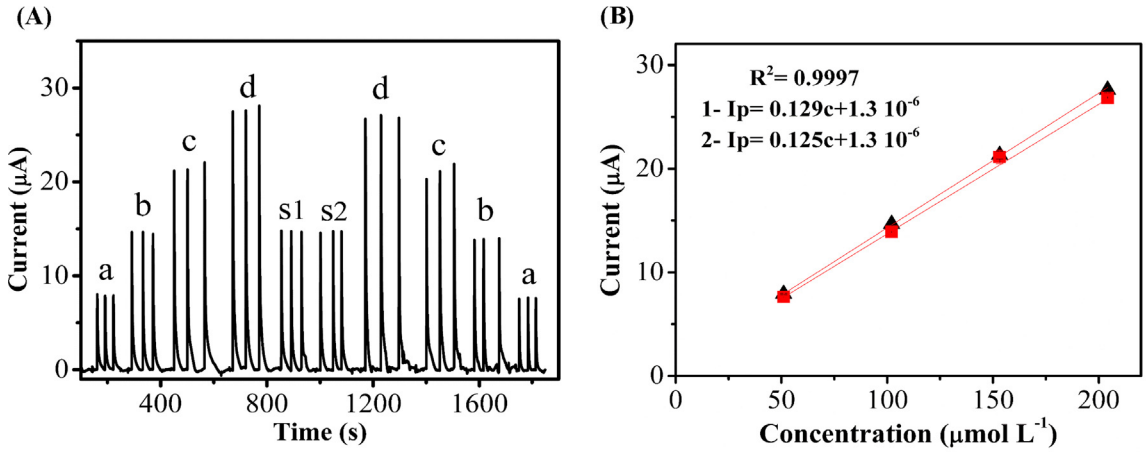

Fig. 7. (A) BIA-amperograms of consecutive injections of four standard solutions of NAC with increasing concentrations (a to d), followed by two different samples of injectable pharmaceutical solution of NAC (S1 and S2), and finally of a new series of injections of the standard solutions but in reverse concentration order (d to a); (B) Calibration curves obtained for the increasing (a to d) and decreasing (d to a) concentration sections shown in (A).

Table 2
Results of analyses carried out in injectable pharmaceutical solutions of NAC.

Samples	Nominal Value (mg mL^{-1})	BIA		HPLC	
		Concentration (mg mL^{-1})	% difference compared with the nominal value	Concentration (mg mL^{-1})	% difference compared with the nominal value
S1	100	104.8 ± 0.4	4.8	106.5 ± 0.4	6.5
S2	100	104.8 ± 0.4	4.8	105.5 ± 0.4	5.5

comparable to those ones obtained by HPLC. The presence of approximately 5% more NAC in the commercial drug is easily justifiable, as the price of this compound is not elevated, and for the manufacturer, is advantageous use more NAC, to compensate for some product degradation. The frequency of analysis achieved using both techniques is a differential aspect that favours BIA. Chromatographic analysis requires 10 min for each analytical run, whereas BIA analysis is performed in only 30 s (i.e. in the time required to analyse one sample by chromatography, it is possible to analyse 20 samples using BIA). In addition, the chromatography generates significantly more waste than BIA. The injectable pharmaceutical products studied here present a very simple composition. The excipients present in both group of ampoules where disodium EDTA, nitrogen gas, sodium hydroxide (for pH adjustment) and water. As water and sodium hydroxide are common in our NAC solutions and nitrogen is an inert gas, only EDTA can be a potential interfering substance. The concentration of EDTA is relatively low compared with that of NAC, and a series of BIA experiments were run with solutions containing only NAC and with NAC + EDTA. The signal recorded for NAC alone (injections of 1×10^{-4} mol L^{-1}) were rigorously the same when a mixture of NAC + EDTA (both 1×10^{-4} mol L^{-1}) was injected in the cell. These results are depicted in Fig. S5 and demonstrate that there were no interfering substances in this study.

4. Conclusions

Small α-$Ni_{0.75}Pb_{0.25}(OH)_2$ NPs approximately 3 nm diameter were prepared, characterized and successfully used for quantitative determination of NAC using an amperometric BIA method. The mixed hydroxide nanoparticles exhibited improved thermal stability and electrochemical properties as compared with $Ni(OH)_2$. A BIA cell with the smallest volume described until now in the literature, with operational volume of only 4 mL, was designed and successfully used in the analyses. The BIA analyses of NAC can be performed in just 30 s (sampling frequency of 120 h^{-1}), compared with the 10 min necessary for each chromatographic analysis (sampling frequency of 6 h^{-1}), at lower cost and generating lower amounts of residue. Furthermore, the new modified electrode presents good sensitivity (calculated detection limit = 0.23 μmol L^{-1}) and no memory effect was confirmed. In addition, the utilization of BIA is much less complex than chromatography, is portable and can be easily applied for quality control of pharmaceutical products.

Acknowledgements

The authors are grateful to the Brazilian agency Conselho Nacional de Desenvolvimento Científico e Tecnológico - CNPq (Processes 163254/2015-2, 402281/2013-6 and 306504-2011-1), and Fundação de Amparo à Pesquisa do Estado de São Paulo - FAPESP (processes 2013/24725-4 and 2015/2076-9) for the financial support and fellowships. JMG thanks to CNPq for his fellowship (process 141853/2015-8).

Appendix A. Supplementary material

Supplementary data associated with this article can be found in the online version at http://dx.doi.org/10.1016/j.talanta.2018.04.053.

References

[1] E. Markoutsa, P. Xu, Redox potential-sensitive N-acetyl cysteine-prodrug nanoparticles inhibit the activation of microglia and improve neuronal survival, Mol. Pharmaceut 14 (2017) 1591–1600.
[2] R.A. Stockley, S.I. Rennard, K. Rabe, B. Celli, Chronic obstructive pulmonary disease: a practical guide to management, John Wiley & Sons, 2008.
[3] P.J. Poole, O.N. Black, Oral mucolytic drugs for exacerbations of chronic obstructive pulmonary disease: systematic review, BMJ 322 (2001) 1271–1274.
[4] Y. Samuni, S. Goldstein, O.M. Dean, M. Berk, The chemistry and biological activities of N-acetylcysteine, Biochim. Biophys. Acta (BBA)-Gen. Subj. 1830 (2013) 4117–4129.
[5] J. Geiler, M. Michaelis, P. Naczk, A. Leutz, K. Langer, H.-W. Doerr, J. Cinatl, N-acetyl-L-cysteine (NAC) inhibits virus replication and expression of pro-inflammatory molecules in A549 cells infected with highly pathogenic H5N1 influenza A virus, Biochem. Pharmacol. 79 (2010) 413–420.
[6] S.M. Talbott, A guide to understanding dietary supplements, Haworth Press, Routledge, 2003.
[7] M. Tepel, M. Van Der Giet, C. Schwarzfeld, U. Laufer, D. Liermann, W. Zidek, Prevention of radiographic-contrast-agent–induced reductions in renal function by acetylcysteine, New Engl. J. Med. 343 (2000) 180–184.
[8] A. Minarini, S. Ferrari, M. Galletti, N. Giambalvo, D. Perrone, G. Rioli, G.M. Galeazzi, N-acetylcysteine in the treatment of psychiatric disorders: current status and future prospects, Expert Opin. Drug Met. 13 (2017) 279–292.
[9] D.N. Seril, J. Liao, K.-L.K. Ho, C.S. Yang, G.-Y. Yang, Inhibition of chronic ulcerative colitis-associated colorectal adenocarcinoma development in a murine model by N-acetylcysteine, Carcinogenesis 23 (2002) 993–1001.
[10] V.I. Sayin, M.X. Ibrahim, E. Larsson, J.A. Nilsson, P. Lindahl, M.O. Bergo, Antioxidants accelerate lung cancer progression in mice, Sci. Transl. Med. 6 (2014) 221ra15.
[11] R.S. Haggag, D.A. Gawad, S.F. Belal, H.M. Elbardisy, Spectrophotometric and spectrofluorimetric determination of mesna, acetylcysteine and timonacic acid through the reaction with acetoxymercuri fluorescein, Anal. Methods-UK 8 (2016) 2479–2493.
[12] M. Rudašová, M. Masár, Precise determination of N-acetylcysteine in pharmaceuticals by microchip electrophoresis, J. Sep. Sci. 39 (2016) 433–439.
[13] A. Zinellu, S. Sotgia, B. Scanu, M.F. Usai, A.G. Fois, V. Spada, A. Deledda, L. Deiana, P. Pirina, C. Carru, Simultaneous detection of N-acetyl-L-cysteine and physiological low molecular mass thiols in plasma by capillary electrophoresis, Amino Acids 37 (2008) 395.
[14] W.T. Suarez, H.J. Vieira, O. Fatibello-Filho, Flow injection turbidimetric determination of acetylcysteine in pharmaceutical formulations using silver nitrate as precipitant reagent, J. Braz. Chem. Soc. 18 (2007) 1028–1033.
[15] B.C. Janegitz, W.T. Suarez, O. Fatibello-Filho, L.H. Marcolino-Junior, Conductometric determination of N-acetylcysteine in pharmaceutical formulations using copper (II) sulphate as titrant, Anal. Lett. 41 (2008) 3264–3271.
[16] S. Sana, A. Rajani, N. Sumedha, P. Pravin, N. Shripad, Development and validation of RP-HPLC method for the estimation of N-acetylcysteine in wet cough syrup, Int. J. Drug Dev. Res. 2 (2012) 284–293.
[17] M.R. Siddiqui, S.M. Wabaidur, M.S. Ola, Z.A. Alothman, M.Z.A. Rafiquee, M.A. Khan, High-throughput UPLC–MS method for the determination of N-Acetyl-L-Cysteine: application in tissue distribution study in wistar Rats, J. Chromatogr. Sci. 54 (2016) 1244–1252.
[18] L.B. Rathod, V. Suvarna, N.K. Shinde, Development and validation of stability indicating RP-HPLC method for simultaneous determination of acetylcysteine and cefexime in pharmaceutical formulation, Int. J. Pharm. Sci. Res. 6 (2015) 4886.
[19] B. Toussaint, C. Pitti, B. Streel, A. Ceccato, P. Hubert, J. Crommen, Quantitative analysis of N-acetylcysteine and its pharmacopeial impurities in a pharmaceutical formulation by liquid chromatography–UV detection–mass spectrometry, J. Chromatogr. A 896 (2000) 191–199.
[20] S.C. Chaves, P.N.C. Aguiar, L.M.F.C. Torres, E.S. Gil, R.C.S. Luz, F.S. Damos, R.A.A. Munoz, E.M. Richter, W.T.P. dos Santos, Simultaneous determination of caffeine, ibuprofen, and paracetamol by flow-injection analysis with multiple-pulse amperometric detection on boron-doped diamond electrode, Electroanalysis 27 (2015) 2785–2791.
[21] A.A. Ensafi, H. Karimi-Maleh, S. Mallakpour, M. Hatami, Simultaneous determination of N-acetylcysteine and acetaminophen by voltammetric method using N-(3,4-dihydroxyphenethyl) – 3,5-dinitrobenzamide modified multiwall carbon nanotubes paste electrode, Sens. Actuators B: Chem. 155 (2011) 464–472.
[22] D. Hernández-Santos, M.B. González-García, A.C. García, Metal-nanoparticles based electroanalysis, Electroanalysis 14 (2002) 1225–1235.
[23] T. Yin, W. Qin, Applications of nanomaterials in potentiometric sensors, TrAC Trends Anal. Chem. 51 (2013) 79–86.
[24] P.R. Martins, L.M.C. Ferreira, K. Araki, L. Angnes, Influence of cobalt content on nanostructured alpha-phase-nickel hydroxide modified electrodes for electrocatalytic oxidation of isoniazid, Sens. Actuat B: Chem. 192 (2014) 601–606.
[25] J.M. Gonçalves, R.R. Guimarães, B.B.N.S. Brandão, L.P.H. Saravia, P.O. Rossini, C.V. Nunes, J.S. Bernardes, M. Berttoti, L. Angnes, K. Araki, Nanostructured Alpha-NiCe mixed hydroxide for highly sensitive amperometric prednisone sensors,

Electrochim. Acta 247 (2017) 30–40.
[26] M.A. Rocha, H. Winnischofer, K. Araki, F.J. Anaissi, H.E. Toma, A new insight on the preparation of stabilized alpha-nickel hydroxide nanoparticles, J. Nanosci. Nanotechno. 11 (2011) 3985–3996.
[27] C.V. Nunes, M. Danczuk, A.A. Bortoti, R.R. Guimarães, J.M. Gonçalves, K. Araki, E.P. Banczek, F.J. Anaissi, Enhanced stability and conductivity of α-$Ni(OH)_2$/smectite clay composites, J. Electrochem. Soc. 163 (2016) A2356–A2361.
[28] M.C. Biesinger, X-ray Photoelectron Spectroscopy (XPS) Reference Pages, Surface Science Western, London, 2015.
[29] D.J. Payne, R.G. Egdell, W. Hao, J.S. Foord, A. Walsh, G.W. Watson, Why is lead dioxide metallic? Chem. Phys. Lett. 411 (2005) 181–185.
[30] M. Dixit, P.V. Kamath, J. Gopalakrishnan, Zinc-substituted α-nickel hydroxide as an electrode material for alkaline secondary cells, J. Electrochem. Soc. 146 (1999) 79–82.
[31] J.M. Goncalves, R.R. Guimaraes, C.V. Nunes, A. Duarte, B.B.N.S. Brandao, H.E. Toma, K. Araki, Electrode materials based on alpha-$NiCo(OH)_2$ and rGO for high performance energy storage devices, RSC ADV 6 (2016) 102504–102512.
[32] A.H. Zimmerman, P.K. Effa, Discharge kinetics of the nickel electrode, J. Electrochem. Soc. 131 (1984) 709–713.
[33] C. Barus, P. Gros, M. Comtat, S. Daunes-Marion, R. Tarroux, Electrochemical behaviour of N-acetyl-L-cysteine on gold electrode—A tentative reaction mechanism, Electrochim. Acta 52 (2007) 7978–7985.
[34] H. Karimi-Maleh, M. Keyvanfard, K. Alizad, M. Fouladgar, H. Beitollahi, A. Mokhtari, F. Gholami-Orimi, Voltammetric determination of N-Actylcysteine using modified multiwall carbon nanotubes paste electrode, J. Electrochem. Sci. 6 (2011) 6141–6150.
[35] M. Fouladgar, H. Karimi-Maleh, R. Hosseinzadeh, Novel nanostructured electrochemical sensor for voltammetric determination of N-acetylcysteine in the presence of high concentrations of tryptophan, Ionics 19 (2013) 665–672.
[36] V. Arabali, H. Karimi-Maleh, H. Beitollahi, R. Moradi, M. Ebrahimi, H. Ahmar, A nanostructure-based electrochemical sensor for square wave voltammetric determination of N-acetylcysteine in pharmaceutical and biological samples, Ionics 21 (2015) 1153–1161.
[37] A. Benvidi, S. Dalirnasab, S. Jahanbani, M.D. Tezerjani, M.M. Ardakani, B.F. Mirjalili, R. Zare, Development of a Carbon Paste Electrode Modified with Reduced Graphene Oxide and an imidazole derivative for simultaneous determination of biological species of N-acetyl-L-cysteine, uric acid and dopamine, Electroanalysis 28 (2016) 1625–1633.
[38] V.S. Santos, V.A. Maraldi, K.S. Bonfim, T.R. Souza, A.P.R. Nakamura, M.S. Magossi, M.S. Magossi, D.S. Fernandes, D.R. Carmo, Voltammetric behavior of zinc Hexacyanoferrate (III) nanoparticles and their application in the detection of N-acetylcysteine, Int. J. Electrochem. Sci. 12 (2017) 7142–7153.
[39] H. Karimi-Maleh, M. Salehi, F. Faghani, Application of novel Ni(II) complex and ZrO2 nanoparticle as mediators for electrocatalytic determination of N-acetylcysteine in drug samples, J. Food Drug Anal. 25 (2017) 1000–1007.
[40] H.R. Zare, F. Chatraei, - Preparation and electrochemical characteristics of electrodeposited acetaminophen on ruthenium oxide nanoparticles and its role as a sensor for simultaneous determination of ascorbic acid, dopamine and N-acetyl-L-cysteine, Sens. Actuators B – Chem. 160 (2011) 1450–1457.
[41] Y. Song, Z. He, H. Hou, W. Xiaolan, W. Li, Architecture of Fe3O4-graphene oxide nanocomposite and its application as a platform for amino acid biosensing, Electrochim. Acta 71 (2012) 58–65.
[42] L.G. Shaidarova, A.V. Gedmina, E.R. Zhaldak, I.A. Chelnokova, G.K. Budnikov, voltammetric determination of acetylcysteine in drugs using an electrode modified by an osmium hexacyanocobaltate film, Pharm. Chem. J. 47 (2014) 48–52.
[43] L. Wang, Y. Ye, Y. Shen, F. Wang, X. Lu, Y. Xie, S. Chen, H. Tan, F. Xu, Y. Song, Hierarchical nanocomposites of Co_3O_4/polyaniline nanowire arrays/reduced graphene oxide sheets for amino acid detection, Sens. Actuators B: Chem. 203 (2014) 864–872.
[44] H.R. Zare, M. Haji-Dehabadi, Z. Shekari, Electrocatalytic oxidation of N-acetyl-L-cysteine at a quercetin multiwall carbon nanotube modified GCE: application for simultaneous determination of ascorbic acid, L-DOPA, N-acetyl-L-cysteine, acetaminophen and tryptophan, Anal. Meth. 7 (2015) 5511–5520.
[45] M.M. Tunesi, R.A. Soomro, R. Ozturk, CuO nanostructures for highly sensitive shape dependent electrocatalytic oxidation of N-acetyl-L-cysteine, J. Electroanal. Chem. 777 (2016) 40–47.
[46] I.S. da Silva, M.F.A. Araujo, H.A. Ferreira, J.D.G. Varela, S.M.C.N. Tanaka, A.A. Tanaka, L. Angnes, Quantification of N-acetylcysteine in pharmaceuticals using cobalt phthalocyanine modified graphite electrodes, Talanta 83 (2011) 1701–1706.
[47] S. Brinic, N. Vladislavic, M. Buzuk, M. Bralic, M. Solic, Bismuth film random array carbon fiber microelectrodes for determination of cysteine and N-acetylcysteine, J. Electroanal. Chem. 705 (2013) 86–90.
[48] S. Nantaphol, O. Chailapakul, W. Siangproh, Ultrasensitive and simple method for determination of N-acetyl-L + -cysteine in drug formulations using a diamond sensor, Electroanalysis 26 (2014) 1024–1030.
[49] M.M. Tunesi, R.A. Soomro, R. Ozturk, The in situ growth of CuO nanostructures on an ITO substrate and its application as a highly sensitive electrode for the electrochemical determination of N-acetyl-L-cysteine, J. Mat. Chem. 5 (2017) 2708–2716.
[50] L. Kukoc-Modun, I. Plazibat, N. Radic, Flow-injection spectrophotometric determination of N-acetyl-L-cysteine based on coupled redox-complexation reaction, Croat. Chem. Acta 84 (2011) 81–86.
[51] L. Kukoc-Modun, D. Tsikas, M. Biocic, N. Radic, Flow-injection analysis of N-acetyl-L-cysteine based on the reduction of copper(II) neocuproine reagent, Anal. Lett. 49 (2016) 607–617.
[52] M.S.M. Quintino, L. Angnes, Batch injection analysis: an almost unexplored powerful tool, Electroanalysis 16 (2004) 513–523.
[53] C. Brett, A.M.O. Brett, L.C. Mitoseriu, Amperometric batch injection analysis: theoretical aspects of current transients and comparison with wall-jet electrodes in continuous flow, Electroanalysis 7 (1995) 225–229.
[54] Farmacopéia Brasileira, in: E.A. LTDA (Ed.), São Paulo, 1988.